Dalton Transactions

ROYAL SOCIETY OF CHEMISTRY

PERSPECTIVE

View Article Online
View Journal | View Issue

Cite this: *Dalton Trans.*, 2025, **54**, 17383

Coke-induced deactivation in zeolite catalysts: mechanisms, anti-coking modifications, and regeneration approaches

Mengdi Zhang, Jing Huang, Fanshuo Meng, Chundong Zhang and Zunmin Zhang *

Received 13th August 2025,
Accepted 13th October 2025

DOI: 10.1039/d5dt01936b

rsc.li/dalton

Zeolite catalysts, widely employed in petrochemical and refining processes, inevitably undergo gradual deactivation. Among the various deactivation pathways, coke-induced deactivation is the most critical, arising from the progressive deposition of carbonaceous species on acid sites and the subsequent blockage of micropores. The characteristics, mechanisms, and kinetics of coke formation are strongly influenced by the zeolite structure, acidity properties, and operating conditions, highlighting the need for a molecular-level understanding to guide catalyst design and regeneration. This review summarizes the recent advances in coke-induced deactivation of zeolite catalysts by covering the mechanisms and physicochemical characteristics of coke formation, strategies for enhancing coke resistance through rational catalyst design, and state-of-the-art regeneration approaches. By bridging fundamental insights and practical strategies, this work aims to support the development of durable zeolite catalysts and efficient regeneration schemes for sustainable industrial applications.

Introduction

Zeolites are crystalline microporous materials characterized by well-defined aluminosilicate frameworks and abundant active sites, which make them archetypal solid acid catalysts in petrochemical and refining processes.[1] The combination of ordered pore architectures, tunable acidity, high hydrothermal stability, and molecular-level shape selectivity enables their extensive use in key acid-catalyzed reactions, such as methanol-to-hydrocarbons (MTH),[2] fluid catalytic cracking (FCC),[3] catalytic pyrolysis of biomass,[4] and methane dehydroaromatization (MDA).[5] The catalytic performance of zeolites originates from the interplay between framework-confined active sites and the spatial constraints imposed by their microporous networks. These two factors jointly determine reaction pathways and product selectivity. Nevertheless, under industrially relevant conditions, zeolite catalysts inevitably experience gradual deactivation, which shortens the catalyst lifetime, reduces the process efficiency and increases operating costs.

Catalyst deactivation represents one of the most persistent challenges in zeolite-based catalysis. It can be broadly defined as the decline in catalytic performance caused by either a reduction in the population of active sites or the loss of their intrinsic functionality during the reaction. From the perspective of reversibility, it is generally categorized as temporary deactivation, exemplified by the coverage of active sites with carbonaceous deposits, and permanent deactivation, such as framework collapse or dealumination. Many intrinsic mechanisms are known to cause zeolite catalyst deactivation, including coke-induced deactivation, poisoning deactivation,[6] hydrothermal degradation, and metal sintering.[7–9] These mechanisms have been reviewed in previous studies.[10–13]

Among them, coke-induced deactivation, also known as carbon deposition, has been identified as the primary cause of zeolite catalyst deactivation in many hydrocarbon conversion reactions.[14] This phenomenon begins with the deposition of carbonaceous species on active acid sites within the zeolite micropores and at pore intersections, progressively covering these active centers. As coke accumulates, it blocks microporous channels, hindering reactant diffusion and ultimately causing a significant decline in catalytic activity.[15,16] However, the mechanisms and kinetics of coke formation strongly depend on the zeolite framework, reaction system, and operating conditions such as temperature, pressure, and feedstock composition. Therefore, understanding the physicochemical characteristics and formation pathways of coke is essential for designing zeolites with enhanced coking resistance and optimizing regeneration strategies for spent catalysts.[17]

Since coke-induced deactivation is typically unavoidable but often reversible, two major strategies have been developed to

State Key Laboratory of Materials-Oriented Chemical Engineering, College of Chemical Engineering, Nanjing Tech University, Nanjing 211816, China. E-mail: zunmin.zhang@njtech.edu.cn

mitigate its effects. The first focuses on the development of long-term coke-resistant catalysts through rational zeolite design, including metal incorporation,[18–20] acidity modulation,[21] and structural modification,[21–24] among other approaches. By fine-tuning the pore topology, the spatial distribution of active sites, and the physicochemical properties, this approach optimizes the balance between catalytic performance and stability. Complementarily, the second strategy emphasizes the implementation of regeneration technologies to restore spent zeolite catalysts. Several methods are commonly employed for coke removal, including oxidative regeneration using air, molecular oxygen (O_2), ozone (O_3), or nitrogen oxides (NO_x),[25] gasification regeneration with carbon dioxide (CO_2) or steam,[26,27] and non-oxidative regeneration approaches under a hydrogen (H_2) or nitrogen (N_2) atmosphere.[28] However, these traditional thermal approaches are often limited by high energy consumption, potential framework degradation, and incomplete coke removal. In recent years, novel techniques such as non-thermal plasma (NTP) regeneration have gained significant attention, as they enable rapid, efficient, and low-temperature coke removal, offering a promising alternative to traditional methods.[29]

While previous reviews have summarized zeolite deactivation and/or regeneration within specific applications,[2,7,8,10,14,15,17,30] this work provides an updated and comprehensive overview of recent advances in coke-induced deactivation of zeolite catalysts. It covers the mechanisms and physicochemical characteristics of coke formation, strategies for enhancing coke resistance through catalyst design, and state-of-the-art regeneration approaches. Our objective is to establish a deeper mechanistic understanding of coke evolution within zeolite frameworks and its role in catalytic deactivation, thereby guiding the development of more durable zeolite catalysts and efficient regeneration schemes for sustainable industrial applications.

Coke-induced deactivation

Coke-induced deactivation remains one of the most critical challenges in zeolite-catalyzed hydrocarbon conversion. It arises from the accumulation of carbonaceous deposits within the zeolite framework, which block microporous channels and cover active sites, leading to a rapid decline in catalytic performance. A thorough understanding of the fundamental mechanisms of coke formation, including its spatial distribution, chemical evolution, and morphological characteristics, is essential for the rational design of anti-coking zeolites and the development of efficient regeneration strategies. A comprehensive analysis of coke-induced deactivation mechanisms in zeolite catalysts is provided in this section.

Characteristics of coke deposition

The chemical composition and structure of coke are closely linked to its formation mechanism and deactivation behavior in zeolite catalysts. Coke is typically characterized as a high-molecular-weight, carbon-rich residue with low volatility and a significantly lower hydrogen-to-carbon (H/C) ratio than the original reactants. Based on their H/C ratio and structural features, coke species are commonly classified into soft coke (higher H/C, mainly aliphatic or olefinic) and hard coke (lower H/C, predominantly aromatic or polyaromatic).[14] These species originate from a series of complex reaction pathways during hydrocarbon processing over zeolites, predominantly involving oligomerization, cyclization, hydrogen transfer, and aromatization. Coke formation is strongly influenced by framework acidity but also by topological confinement, and catalyst deactivation primarily occurs *via* micropore blockage and active site coverage.

In zeolite-catalyzed systems, Brønsted (BAS) and Lewis (LAS) acid sites act simultaneously as catalytic centers and as nucleation sites for coke formation. The relative contributions of these sites to coke formation differ significantly between metal-free and metal-loaded catalysts. Consequently, coke species are commonly classified according to their associated acid sites, with aliphatic C_xH_y deposits predominantly linked to LAS and polycyclic aromatic hydrocarbons to BAS.[14,31] The intrinsic coupling between catalytic activity and deactivation ultimately governs catalyst stability and lifetime. When hydrocarbons interact with these acid or metal sites at elevated temperatures, progressive carbon deposition initially leads to partial coverage of the active centers and, upon continued growth, to their complete encapsulation. In parallel, the accumulation of larger coke species within the microporous network induces severe pore blockage, imposing mass-transfer limitations and further accelerating catalyst deactivation.

The strength, density, and spatial distribution of acid sites critically influence the pathways and extent of coke formation. In general, strong Brønsted and Lewis acid sites simultaneously function as catalytic centers and preferential loci for coke nucleation. Díaz *et al.*[32] demonstrated that during the oligomerization of 1-butene, the HZ-30 zeolite (HZSM-5, SiO_2/Al_2O_3 = 30), possessing the highest Brønsted acid site density among the tested samples, generated 6.21 wt% of hard coke. In contrast, the high-silica samples HZ-80 and HZ-280 (SiO_2/Al_2O_3 = 80 and 280, respectively) mainly formed loosely bound soft coke near Lewis acid sites, with a significantly reduced amount of hard coke compared to HZ-30. However, when the acid strength and density exceed the optimal range, coke formation is greatly accelerated. For example, Wan *et al.*[33] demonstrated that decreasing the SiO_2/Al_2O_3 ratio from 217 to 23 in nanocrystal ZSM-5 catalysts increased the acid site density, leading to markedly higher coke formation and faster catalyst deactivation, while the moderate acid density sample maintained sustained activity with minimal coke deposition. Moreover, extending beyond total acidity, the strong/weak acid site ratio is more critical than the total acid amount. Moreover, Bedenko *et al.*[34] demonstrated that H-MFI (ZSM-5, MFI framework), despite possessing 60% higher total acidity than H-BEA (Beta zeolite), exhibited a strong/weak acid site ratio of 0.60 *versus* 0.25, resulting in a fourfold faster deactivation rate and significantly shorter catalyst lifetime. Collectively, these find-

ings highlight that rational zeolite catalyst design requires precise acidity tuning, particularly optimizing the strong/weak acid site ratio, to balance activity, selectivity, and stability.

In addition to acidity, the structural characteristics of zeolites, including pore size, channel topology, and void geometry, play a critical role in governing coke formation, distribution, and catalyst deactivation. While acidity determines the chemical nature and nucleation of coke species, the physical framework controls their spatial confinement, diffusion, and preferred accumulation sites.

Zeolite pore size is a fundamental determinant of the coke molecular structure, primarily through spatial confinement effects that sterically control which coke precursors can form and grow within the microporous framework. Castaño *et al.*[35] demonstrated that during high-density polyethylene cracking, HZSM-5 with medium-pore MFI topology (10-MR) accumulated the lowest coke content dominated by branched aliphatic fragments and short alkyl aromatics, whereas the larger-pore Hβ and HY (12 ~ MR) facilitated extensive hydrogen transfer and aromatic condensation, yielding highly polycondensed aromatic coke that rapidly blocked micropores, as shown in Fig. 1a. This pore size-dependent selectivity arises because medium pores sterically restrict the growth of bulky polyaromatic species, while large pores provide sufficient space for progressive aromatic condensation and multiple hydrogen transfer reactions that lead to highly condensed coke structures.

Beyond pore size, framework topology governs the spatial distribution and speciation of coke through its control over void geometry and preferential coking sites within micropore networks. Recent powder neutron diffraction and spectroscopic analysis by Rzepka *et al.*[36] demonstrated that the largest void zones act as preferential coking sites, and topology-dependent void geometry governs where coke accumulates: in MFI, coke is confined at 10 MR intersections as tricyclic anthracene-like species; in FER, alkyl-substituted benzenes concentrate at 8 × 10 MR junctions; while in CHA (SSZ-13), naphthalene- and pyrene-type aromatics populate large cages and even bridge across 8 MR windows, as shown in Fig. 1b. These distinct microenvironments selectively stabilize coke species based on the shape-selective fit between molecular geometry and void architecture, illustrating that topology effects extend beyond simple pore size considerations.

Channel dimensionality and connectivity represent additional critical aspects of framework topology that profoundly influence coke distribution patterns and deactivation kinetics. Migliori *et al.*[37] reported that in methanol-to-DME conversion FER and MFI frameworks with 2-D or 3-D intersecting channels predominantly formed light monocyclic aromatics confined within micropores, while MOR with one-dimensional 12-ring channels promoted the condensation of bulky polycyclic aromatic clusters on the external surface, leading to the fastest deactivation and complete acid site coverage (Fig. 2a). Similarly, Chen *et al.*[18] showed that in one-dimensional MOR, toluene-derived species accumulate mainly at pore mouths and external surfaces rather than within micropores, causing rapid blockage and poor regenerability. Wennmacher *et al.*[38] revealed that in ZSM-5 during methanol-to-hydrocarbon conversion coke nucleation initiates at channel intersections and progressively condenses through straight micropores, which retain nearly twice the coke content of sinusoidal channels at advanced deactivation stages, as shown in Fig. 2b. Collectively, these observations indicate that multi-dimensional, well-connected channel systems provide multiple diffusion pathways and more uniform coke distribution, whereas one-dimensional frameworks are highly susceptible to rapid deactivation once pore mouth coking occurs.

Hierarchical modification, achieved by introducing secondary mesopores and macropores, fundamentally reshapes coke formation and catalyst deactivation by alleviating pore size and connectivity constraints imposed by conventional microporous frameworks.[22] This architecture improves the accessibility of bulky hydrocarbons to internal acid sites and facilitates transport and combustion of coke species during regeneration. In a series of studies, Fals *et al.*[39–42] showed that hierarchical Y zeolites with enhanced mesoporosity, such as Y-0.20-S (Y zeolite treated with 0.20 mol L^{-1} NaOH and subsequently steamed),

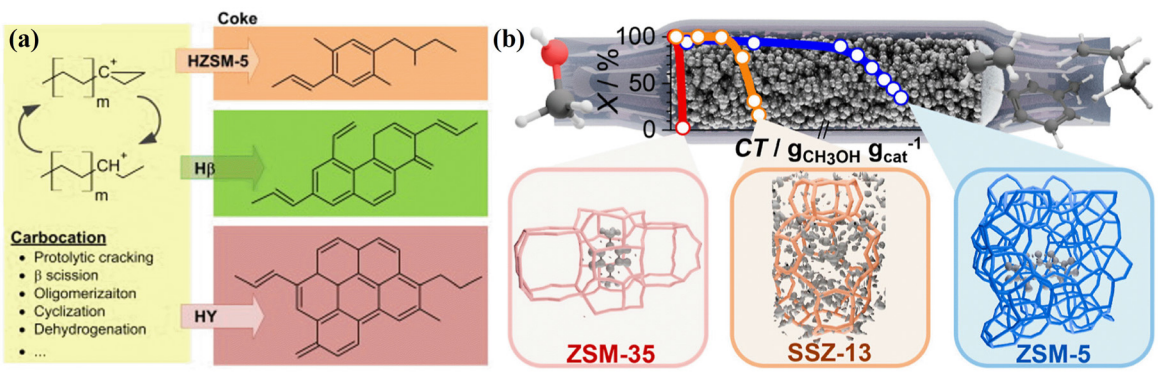

Fig. 1 (a) Representative coke molecule formed on HZSM-5, Hβ, and HY zeolite catalysts during polyethylene cracking, reproduced from ref. 35 with permission from Elsevier, copyright 2011. (b) Visualization of the coke distribution in ZSM 5 (MFI), ZSM 35 (FER), and SSZ 13 (CHA) during methanol-to-hydrocarbon conversion, reproduced from ref. 36 with permission from American Chemical Society, copyright 2024.

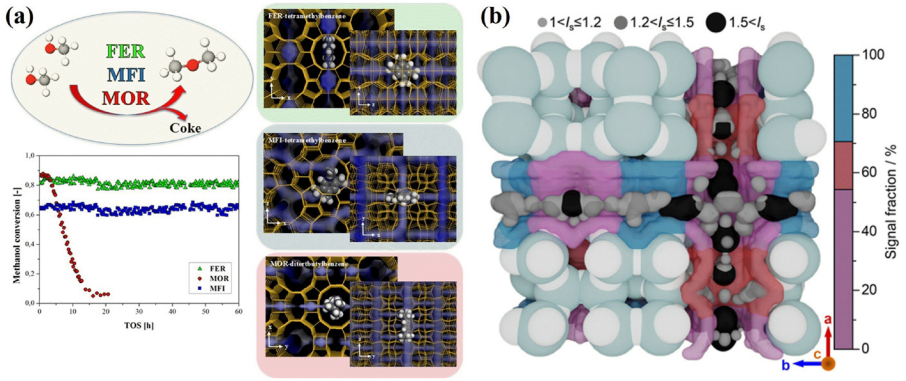

Fig. 2 (a) Coke deposition patterns in the methanol-to-DME reaction over MOR, MFI, and FER zeolites, reproduced from ref. 37 with permission from Elsevier, copyright 2018. (b) Distribution of the coke-associated signal in the zeolite unit cell as extracted from the direct electron diffraction maps of the severely-coked ZSM-5 catalyst, reproduced from ref. 38 with permission from Wiley, copyright 2022.

exhibited higher coke selectivity but maintained superior catalytic stability over multiple cracking and regeneration cycles. This was attributed to the preferential accumulation of highly condensed aromatic coke in mesopores, which facilitated its removal during regeneration and preserved access to active sites. The anti-coking advantages of such structural modifications are discussed later in detail in this review.

Deactivation mechanism and kinetics

Coke formation on zeolite catalysts is a complex, system-specific process that varies significantly with reaction environment conditions and catalyst composition. Typically, the coke-induced deactivation of zeolites proceeds through two sequential steps,[43] as illustrated in Fig. 3. In the initial stage, carbonaceous species deposit on the catalyst surface and progressively cover the active sites. At elevated temperatures, hydrocarbon molecules are adsorbed onto Brønsted acid sites, Lewis acid sites, or supported metal sites through either monolayer chemisorption or multilayer physisorption. These adsorbed species undergo stepwise oligomerization, generating carbon-rich intermediates (C_xH_y fragments). As coke continues to accumulate, it encapsulates active sites, resulting in a loss of catalytic function. In the subsequent stage, coke deposits build up within micropores, which hinders molecular diffusion and further accelerates deactivation by restricting reactant access and product transport.

The kinetics of coke formation also exhibit distinct patterns that strongly depend on the reaction type, operating conditions, and zeolite characteristics. Typically, the coking rate shows a rapid initial increase followed by a gradual decline as active sites become progressively blocked. For instance, in a

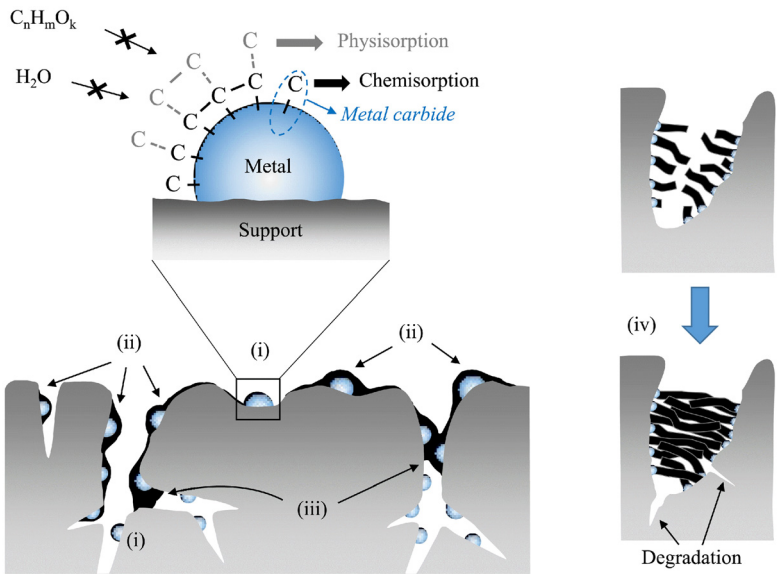

Fig. 3 Schematic illustration of coke-induced deactivation pathways occurring at the active sites (metals) and within the porous structures of supported catalysts, reproduced from ref. 43 with permission from Elsevier, copyright 2019.

kinetics study of coke formation in the dimethyl ether-to-olefin process over SAPO-34, Gao *et al.*[44] revealed a three-stage autocatalytic pathway in which the coking rate initially increases with coke content, reaches a maximum when autocatalytic promotion counterbalances active site consumption, and subsequently declines rapidly as catalyst deactivation dominates. During catalytic cracking over β-zeolites, Zhou *et al.*[45] reported a similar kinetic behavior but without the autocatalytic feature. These kinetic profiles reflect the coupling between coke chemistry, active site accessibility, and diffusional constraints in the porous framework. Building on these insights, the development of accurate deactivation models is indispensable for translating these complex mechanistic and kinetic understandings into predictive tools for process design and control, with the aim of maximizing catalyst utilization and sustaining the catalytic performance. This has been well established in recent specialized literature.[46–48]

In addition, temperature plays a critical role by modifying the kinetics and thermodynamics of coke-forming reactions through interactions with catalyst properties and other process conditions. It exhibits distinct threshold and non-linear effects where increasing temperature not only accelerates coke formation, but also alters its nature and spatial distribution. In MTH, the catalyst lifetime declines sharply above 673 K as coke evolves from surface-dispersed species to micropore-confined polycyclic aromatics.[49] In biomass fast pyrolysis, the coke content reaches 52.3% at 400 °C and decreases at higher temperatures, accompanied by a shift from surface to micropore deposition.[50] Pressure also affects the evolution of carbon deposits. Díaz *et al.*[32] demonstrated that during 1-butene oligomerization over HZSM-5, higher pressure markedly promotes the formation and accumulation of soft coke while suppressing the development of hard coke. This behavior was attributed to the reduced concentration of light reactants under high-pressure conditions and the physical hindrance exerted by the soft coke layer on the subsequent growth of hard coke.

Anti-coking modifications

Catalyst deactivation through coke formation represents a fundamental challenge in zeolite-catalyzed industrial processes, directly impacting both process economics and operational efficiency. While regeneration technologies can restore catalytic activity after deactivation, preventive anti-coking strategies provide greater economic benefits by extending the catalyst lifespan and reducing the regeneration frequency. Recent advances in the rational design of anti-coking zeolite catalysts are reviewed herein, focusing on three major approaches: metal incorporation, acidity modulation, and structure engineering.

Metal incorporation

In recent years, metal-in-zeolite catalysts have experienced rapid development and gained widespread application in heterogeneous catalysis, particularly through the incorporation of metal species at various structural positions. While certain metals (*e.g.*, Ti, Sn, Ga) can occupy framework tetrahedral sites as isolated atoms, most transition and noble metals are introduced as extra-framework species, including isolated cations, single atoms, subnanometric clusters, and nanoparticles confined within zeolite channels and cages.[51,52] Such strategic metal incorporation has been demonstrated to substantially enhance the catalytic activity and selectivity, while simultaneously improving the structural stability and resistance to deactivation.[53,54]

A wide range of metal species have been successfully incorporated into zeolites at these various positions, including transition metals (Mo, Fe, Co, Ni), noble metals (Pt, Au, Ag), and main-group metals (Ga, Zn, In), with the majority occupying extra-framework sites. This metal incorporation results in improved catalytic activity and selectivity as well as enhanced resistance to coke-induced deactivation.[14] Both the choice of metal, its structural position and the precise control of loading are critical in determining the catalyst performance, with the optimal parameters varying substantially across different reactions and application systems.

This strong dependence arises from the fundamental roles of metal species and loading levels in modulating the physicochemical properties of zeolite catalysts. Different metals can alter the balance between Brønsted and Lewis acid sites, modify the reaction selectivity and product distribution, and influence the nature and location of coke deposits, thereby steering reaction pathways and catalytic stability. Meanwhile, metal loading affects active site dispersion, pore accessibility, and the extent of acid site modification: low-level doping often optimizes acidity and suppresses coke precursors, whereas excessive loading can lead to particle aggregation, pore blockage, and accelerated deactivation.

For example, Sedighi *et al.*[55] systematically compared SAPO-34 modified with different metal ions (Fe, Co, Ni, La, Ce). The metals were predominantly located at extra-framework positions with minor framework substitution. Rare-earth incorporation, particularly Ce and La, significantly extended the catalyst lifetime and suppressed coke formation in methanol-to-olefins (MTO) compared to both parent and transition-metal-modified SAPO-34, as shown in Fig. 4a. The improved performance was attributed to reduced acidity resulting from hindered Si incorporation and the modified acid site distribution. Yao *et al.*[56] showed that wet impregnation-prepared Co- and Mo-modified ZSM-5 (1 wt% Co and 3 wt% Mo, respectively) increased light aromatic yields from cellulose catalytic fast pyrolysis at 600 °C and reduced coke amounts compared to parent ZSM-5. However, catalyst deactivation was dictated more by the coke morphology and location than by the total yield, with Mo sites favoring disordered polyaromatic species and Co sites promoting graphite-like carbon. Anekwe *et al.*[57] demonstrated that low-level (0.5 wt%) Co, Fe, or Ni doping of ZSM-5 optimized the acidity and ethanol-to-hydrocarbon selectivity, whereas excessive loading (10 wt%) promoted coke deposition and accelerated deactivation, highlighting the critical role of precise metal loading in anti-coking design.

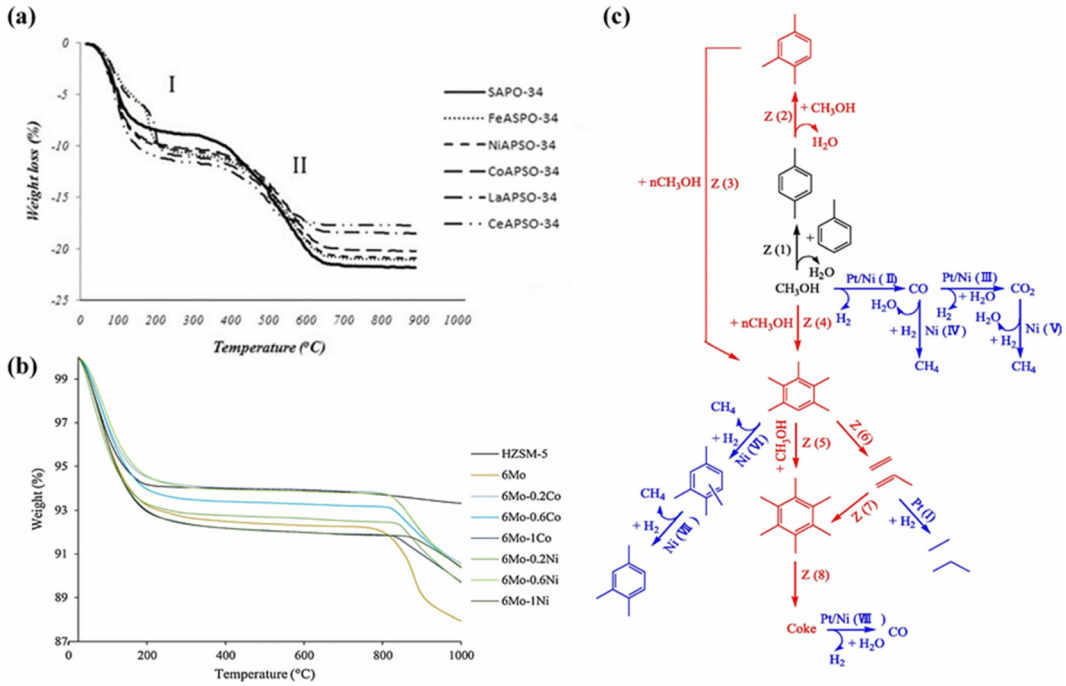

Fig. 4 (a) TGA plots for discharged SAPO-34 and MeAPSO-34, reproduced from ref. 55 with permission from Elsevier, copyright 2015. (b) TGA plots for all fresh as-synthesized catalysts before receiving any type pretreatment, reproduced from ref. 58 with permission from Elsevier, copyright 2019. (c) Proposed reaction pathways of shape-selective alkylation of toluene with methanol over Pt and/or Ni loaded ZSM-5 catalyst, reproduced from ref. 59 with permission from Elsevier, copyright 2022.

Recently, bimetallic zeolite catalysts have attracted significant attention.[58–66] The addition of a second metal can enhance the stability of the active component by inhibiting sintering and reducing coke formation, while synergistic interactions between the metals improve the catalytic activity and modify the product selectivity. Moreover, precise control of the metal ratio has been demonstrated as a key factor in optimizing the anti-coking performance across diverse hydrocarbon conversion processes. For example, in MDA at 700 °C and atmospheric pressure, Co-Mo/ZSM-5 catalysts exhibited optimal anti-coking behavior at 0.6 wt% Co loading, significantly reducing coke deposition and catalyst deactivation compared to monometallic Mo/ZSM-5,[58] as shown in Fig. 4b. Han *et al.*[59] identified unique advantages of the (Pt + Ni)/ZSM-5 zeolite: Pt and Ni play distinct roles in suppressing the coke precursor (*e.g.*, light olefins) formation—Pt hydrogenates olefins to alkanes, while Ni inhibits olefin generation by promoting methanol dehydrogenation and methane formation. Compared to ZSM-5 with Pt or Ni alone, the Pt–Ni co-loaded catalyst shows significantly enhanced coke resistance and stability in toluene–methanol alkylation, offering a new strategy to mitigate coking, as shown in Fig. 4c. Similarly, ZnCo/ZSM-5 catalysts achieved high paraffin conversion and selective BTX(benzene, toluene, and xylene) production, where the Zn/Co synergy balanced the Brønsted–Lewis acidity and suppressed coke formation.[60] Comparable improvements were reported in CO_2 hydrogenation with Fe-Co/HZSM-5 tandem catalysts, which promoted gasoline-range hydrocarbon formation and mitigated coke-induced deactivation *via* the optimized Fe/Co ratios and acidity.[61] In lignite tar upgrading, Co/Ce bimetallic ZSM-5@activated carbon catalysts demonstrated enhanced yields of benzene, toluene, ethylbenzene, xylene, and naphthalene and regeneration stability, attributed to the metal synergy and hierarchical carbon supports that improved dispersion and coke resistance.[62] Khezri *et al.*[63] reported that Ce–Ca–HZSM 5 nanoparticles exhibited markedly reduced coke deposition (TGA weight loss ~4% *vs.* 19% for parent HZSM-5) and enhanced long-term stability in MTO, highlighting the synergistic effect of rare-earth and alkaline-earth metal modification in suppressing coking and tuning acidity.

Despite these successful applications, the development of desired metal-loaded zeolite catalysts continues to pose a significant challenge. Several critical issues must be carefully addressed to achieve optimal catalytic performance and long-term coke resistance. First, the selection of metal species is crucial, as not all metals are suitable for specific reactions. For instance, Mo-loaded zeolites often suffer from metal migration and sintering, resulting in irreversible deactivation,[67] while conventional Fe-impregnated zeolite catalysts suffer from rapid deactivation due to complete carburization of iron species, accompanied by severe coking and prolonged induction periods.[68] Similarly, Ni-doped HZSM-5 catalysts exhibit obvious deactivation in ethanol-to-hydrocarbon conversion due to enhanced coke deposition and pore blockage caused by Ni species.[69]

Second, precise control of metal loading is essential, as excessive amounts can induce particle agglomeration, pore

blockage, and accelerated coke accumulation. Third, achieving uniform metal dispersion is fundamental for maximizing the active site accessibility and suppressing coke precursors. To this end, various advanced preparation techniques have been developed to enhance dispersion and stabilize active species, including supercritical solvent impregnation, ultrasonic-assisted ion exchange, and intracrystalline metal encapsulation.[14] Altogether, these challenges highlight the need for rational catalyst design that integrates metal–acid synergy, structural stability, and coke-suppression mechanisms.

Acid modulation

Acidity modulation focuses on the fundamental catalytic sites responsible for both desired reactions and undesired coke precursor formation. This approach involves systematic tuning of the density, strength, type, spatial distribution, and accessibility of Brønsted and Lewis acid sites in zeolite frameworks through various chemical and physical treatments.[70–73] Brønsted acid sites (Si–OH–Al bridging hydroxyls) predominantly mediate proton-transfer and carbocation-mediated chain reactions, whereas Lewis acid sites (coordinatively unsaturated Al^{3+} or extra-framework species) promote electron-pair acceptance and hydride abstraction pathways. The balance between Brønsted and Lewis acidity, their strength distribution, and spatial proximity critically determine the reaction selectivity, activity, and, most importantly, coke formation propensity.

The silicon-to-aluminum ratio (Si/Al) is a fundamental structural parameter governing zeolite acidity and, consequently, anti-coking performance. Sanhoob *et al.*[74] evaluated ZSM-5 catalysts with Si/Al ratios ranging from 30 to 1200 in the MTO reaction and observed that the ethylene selectivity decreased while the propylene selectivity increased with higher Si/Al ratios, with the catalyst lifetime peaking at 33 h for Si/Al = 150, as shown in Fig. 5a. Similarly, Huang *et al.*[75] investigated H-ZSM-5 with Si/Al ratios between 50 and 4000 for methanol-to-propylene conversion and found that the propylene selectivity increased monotonically, reaching a maximum of 58.91% at Si/Al = 1600 under full methanol conversion. This trend was attributed to a shift in the dominant reaction pathway from arene-based methylation/dealkylation to alkene-based methylation/cracking, driven by the reduced acid site density and weakened acidity, which suppress hydrogen transfer and cyclization, the key steps in coke precursor formation. However, excessively high Si/Al ratios (>1600) result in insufficient acid sites and loss of activity, indicating that an optimal Si/Al ratio is required to balance catalytic activity, selectivity, and coke resistance.

Multiple strategies for acidity modification, including chemical acid treatments and site-specific surface engineering, provide versatile approaches to tailor the catalytic behavior and coke resistance of zeolites. Degirmencioglu *et al.*[76] systematically investigated the effects of phosphoric, sulfuric, and hydrochloric acid treatments on HZSM-5 in the methanol-to-olefin reaction and demonstrated that phosphoric acid treatment produced the highest light olefin selectivity and the lowest coke formation (Fig. 5b). This effect was attributed to the formation of a SAPO-like structure, which moderated acidity and extended the catalyst lifetime. In another study,

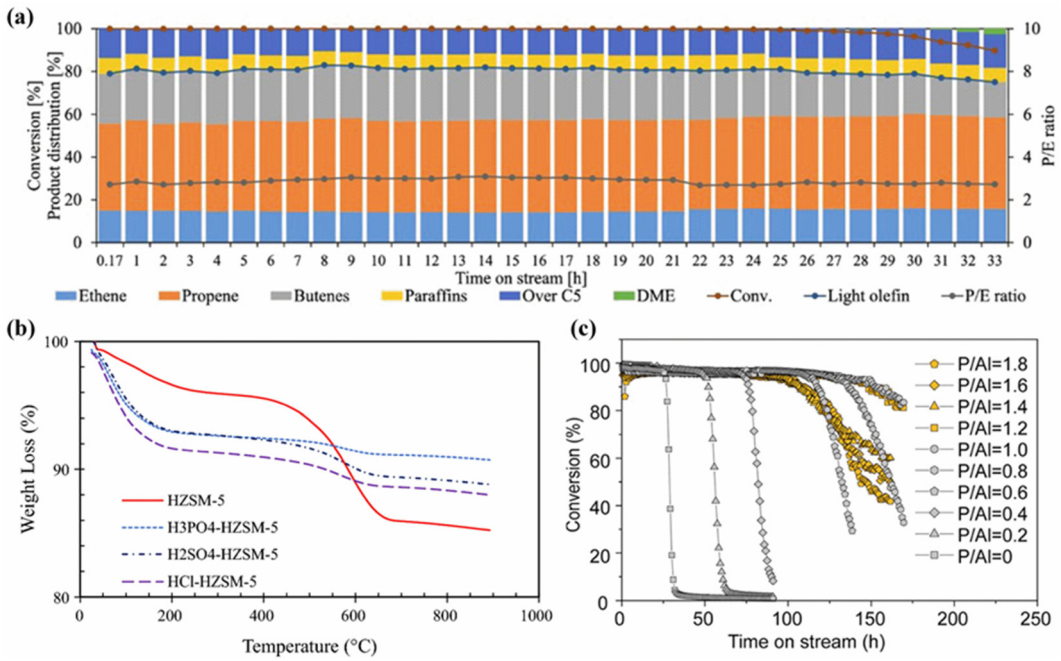

Fig. 5 (a) Catalytic methanol conversion to olefin over the modified ZSM-5 zeolite, reproduced from ref. 74 with permission from Springer Nature, copyright 2023. (b) TGA profiles of the spent HZSM-5, H_3PO_4-HZSM-5, H_2SO_4-HZSM-5, and HCl-HZSM-5 catalysts, reproduced from ref. 76 with permission from Springer Nature, copyright 2023. (c) Catalytic performance of ZSM-5 and P-ZSM-5 catalysts at 400 °C with a WHSV of 16 h^{-1}, reproduced from ref. 78 with permission from American Chemical Society, copyright 2025.

Gan *et al.*[77] reported that precise tuning of acid properties in Mo/HZSM-5 is critical for MDA. Introducing Ce promoters optimized the strong-to-weak Brønsted acid ratio, increasing the aromatic selectivity from 58% to 75% and reducing coke formation, while passivating external acid sites *via* Silicalite-1 coating decreased the deactivation rate from 0.22 h^{-1} to 0.06 h^{-1} by suppressing polyaromatic coke precursors and enhancing Mo dispersion. Altogether, these results highlight how targeted control of acid strength and spatial distribution can synergistically enhance the catalytic performance while mitigating coke deposition.

Phosphorus modification is another versatile strategy for fine-tuning the zeolite acidity and enhancing the anti-coking performance, aluminum-specific coordination and formation of local silicoaluminophosphate (SAPO) interfaces.[78–83] Phosphorus modification simultaneously moderates acid strength, adjusts the acid site density, and alters pore diffusion properties through Al–O–P bond formation at framework aluminium sites and the deposition of polyphosphate species. Song *et al.*[78] demonstrated in ZSM-5 that ammonium phosphate treatment systematically reduced strong Brønsted acid sites (236 → 53 μmol g^{-1} at P/Al = 1.6) while generating weak acid sites. The formation of local SAPO interfaces at distorted framework aluminum sites suppressed coke precursor formation and extended the catalyst lifetime from 25 h to 149 h (at P/Al = 1.0, approximately 6-fold), as shown in Fig. 5c. Solid-state NMR confirmed that polyphosphate species coordinate with framework AI and react with extra-framework Al, retarding the growth of naphthalene and polyaromatic species. Operando UV–vis analysis further revealed the delayed kinetics of polyaromatic formation, attributed to the suppression of the 1,2,3-trimethylcyclopentenyl cation—a key intermediate in both the hydrocarbon pool mechanism and coke formation pathway. Lee *et al.*[80] observed similar effects in SSZ-13, where phosphorus impregnation weakened acidity *via* Al–O–P linkages and partially blocked pore mouths, reducing the diffusion of bulky hydrocarbons and selectively suppressing the 1,2,3-trimethylcyclopentenyl cation associated with the alkyl naphthalene hydrocarbon pool mechanism. Al-Shafei *et al.*[81] reported that in nano-Y zeolite 2 wt% P_2O_5 incorporation created new weak acid sites while moderating strong acid sites, shifting the acid strength distribution toward optimal values for selective steam cracking of *n*-dodecane and achieving a 23% higher light olefin yield. X-ray photoelectron spectroscopy confirmed Al–O–P bond formation that stabilizes the framework and enhances the Lewis acidity. Collectively, these studies establish phosphorus modification as a multi-dimensional acidity engineering approach integrating aluminum-specific coordination, acid site tuning, diffusion control, and coke suppression into a single synergistic strategy.

Structure engineering

While metal loading and acidity modulation primarily tailor the chemical properties of zeolites by adjusting active sites and directing catalytic pathways, structural engineering provides a complementary strategy by constructing hierarchical pore architectures that integrate intrinsic micropores with auxiliary meso- and macropores. These hierarchical structures enhance the catalytic performance by improving active site accessibility and facilitating mass transport, providing unobstructed pathways for bulky intermediates and coke precursors while preserving the intrinsic catalytic functionality of the microporous framework. As a result, improved diffusion mitigates internal coke formation, prolongs the catalyst lifetime, and enables more efficient regeneration.[22,84,85] These benefits underpin the broad applicability of hierarchical zeolites in various catalytic processes and contribute to improved utilization efficiency alongside reductions in energy, time, and raw material consumption in industrial operations.

Recent advances in hierarchically structured zeolites have demonstrated remarkable improvements in both catalytic performance and coke resistance across diverse reactions.[39–42,86–90] In methanol-to-gasoline conversion, hierarchical MFI zeolite nanosheets with 2 nm thickness exhibited an extended catalyst lifetime with a dramatically reduced coke deposition rate (45 mg g^{-1}) compared to conventional MFI zeolites (170 mg g^{-1}), as the coke formed mainly at the mesopore surface while conventional MFI zeolites showed coke formation inside the micropores.[86] In methanol-to-olefin reactions, hierarchical SAPO-34 zeolites with tailored micropore–mesopore–macropore architectures achieved a prolonged lifetime of 206 min and an ethylene + propylene selectivity of 84.35%, markedly outperforming conventional microporous SAPO-34 (106 min, 77.53%) owing to shortened diffusion pathways and enhanced diffusion facilitated by interconnected pores and thin walls.[87] Mechanistic studies revealed that introducing hierarchical structures with interconnected mesopores significantly reduced the diffusion resistance by a factor of five and increased the diffusion coefficient by two orders of magnitude, shifting the rate-determining step from micropore diffusion to acid-site adsorption while alleviating coke deposition near pore mouths,[88] as shown in Fig. 6a.

In catalytic fast pyrolysis of biomass, desilicated hierarchical ZSM-5 zeolites facilitated the diffusion of bulky lignin-derived oxygenates, producing higher aromatic hydrocarbon yields (30.2% *vs.* 23.2%) and reduced coke formation (39.9% *vs.* 44.4%) compared to parent ZSM-5, with optimal performance achieved under mild alkaline treatment.[89] Similarly, Sun *et al.*[90] synthesised SAPO-34 aggregates with hierarchical structures assisted by an organosilane and studied their performance in the MTO reaction. The hierarchical structure not only enhances the diffusion performance of the catalyst, but also reduces the formation of coke (Fig. 6b), thereby prolonging the catalyst lifetime and improving the selectivity to light olefins. Collectively, these examples illustrate that hierarchical porosity, realized through thin-walled or nanosheet morphologies, micro–meso–macroporous architectures, and interconnected pore networks, effectively mitigates coke-induced deactivation. These features synergistically enhance mass transport, prevent the accumulation of coke precursors into heavy, deactivating species, and preserve micropore accessibility for catalytic reactions.

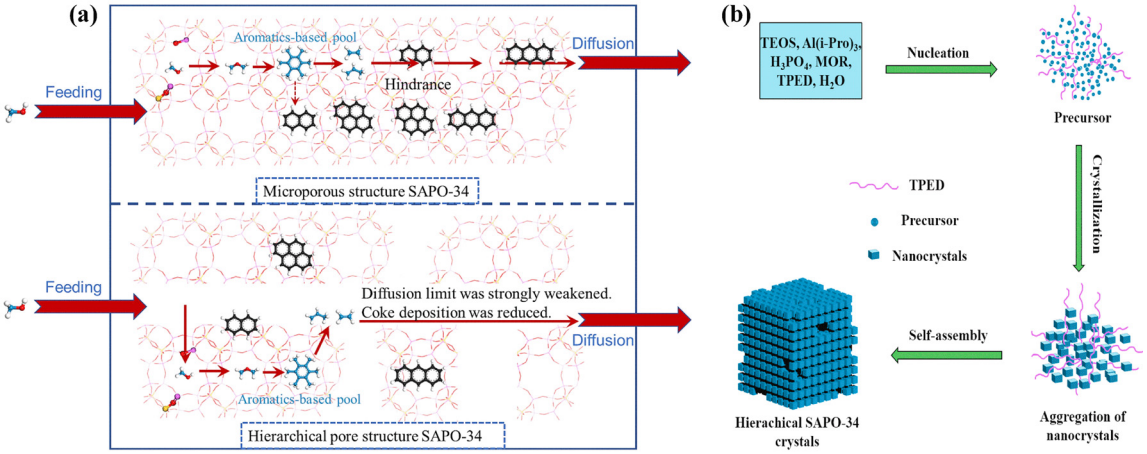

Fig. 6 (a) Mechanism of the reaction–diffusion process in the hierarchical pore structure SAPO-34, reproduced from ref. 88 with permission from Elsevier, copyright 2024. (b) Schematic illustration of the crystallization process of hierarchical SAPO-34 aggregates assisted by the organosilane, reproduced from ref. 90 with permission from Elsevier, copyright 2021.

Extensive studies on hierarchically porous zeolites have elucidated key mechanisms by which tailored pore architectures alleviate coke-induced deactivation across diverse catalytic systems. A consistent observation is the redistribution of coke deposits from micropore interiors to mesopore surfaces and external crystal interfaces. This behavior arises from enhanced mass transport and shortened diffusion pathways, which enable rapid removal of coke precursors and prevent their accumulation into heavy, deactivating species. Such effects have been demonstrated across various zeolite frameworks, resulting in reduced coke buildup and significantly extended catalyst lifetimes. Moreover, catalytic improvements strongly correlate with mesopore connectivity, as open, interconnected pore networks consistently outperform structures containing isolated intracrystalline voids. Overall, these insights highlight hierarchical porosity as a versatile design strategy that modulates coke formation kinetics and improves the catalyst durability.

Regeneration approaches

Although anti-coking modifications can effectively mitigate catalyst deactivation, coke formation remains inevitable during long-term operation. Regeneration thus serves as a critical complementary strategy to restore the catalytic performance by removing carbonaceous deposits, reactivating active sites, and preserving structural integrity.[7,15,91] Conventional methods, including oxidative combustion, gasification, and hydrogenation, are widely employed but often involve high thermal stress, incomplete decoking, and potential structural degradation of the zeolite framework. Recent efforts have been focused on developing more selective, energy-efficient, and less destructive alternatives. The following subsections review representative regeneration strategies for zeolite-based catalysts, emphasizing their mechanisms, performance, and practical applicability.

Oxidative regeneration

Oxidative regeneration is the most widely adopted strategy for removing coke deposits from deactivated zeolite catalysts owing to its simplicity, efficiency, and industrial scalability. It involves combusting carbonaceous species with air or pure oxygen at elevated temperatures, typically in the range of 450 °C to 600 °C. The method is extensively applied in industrial processes such as FCC[92] and MTO,[93] which commonly experience coke-induced catalyst deactivation. The regeneration process is highly exothermic and governed by a series of well-defined oxidation reactions involving hydrogen, carbon, and carbon monoxide:[15,94]

$$2H(s) + \frac{1}{2}O_2(g) \rightarrow H_2O(g), -121.0\ \text{kJ mol}^{-1} \quad (1)$$

$$C(s) + \frac{1}{2}O_2(g) \rightarrow CO_2(g), -395.4\ \text{kJ mol}^{-1} \quad (2)$$

$$C(s) + \frac{1}{2}O_2(g) \rightarrow CO(g), -110.4\ \text{kJ mol}^{-1} \quad (3)$$

$$CO(g) + O_2(g) \rightarrow CO_2(g), -285.0\ \text{kJ mol}^{-1} \quad (4)$$

These reactions provide the thermodynamic foundation for coke removal and determine the heat balance during regeneration.

The pore architecture and framework topology of zeolite crystals play a decisive role in governing the kinetics and mechanism of coke oxidation during regeneration. Magnoux *et al.*[95] demonstrated that large-pore zeolites such as HY and H-mordenite consistently exhibited faster regeneration rates than medium-pore analogues like HZSM-5, primarily due to enhanced oxygen diffusion and improved oxygen–coke accessibility afforded by the large-pore architecture. A comparative study of HFAU and HEMT zeolites further highlighted the crucial role of framework topology in controlling the regeneration efficiency through its influence on coke deposition

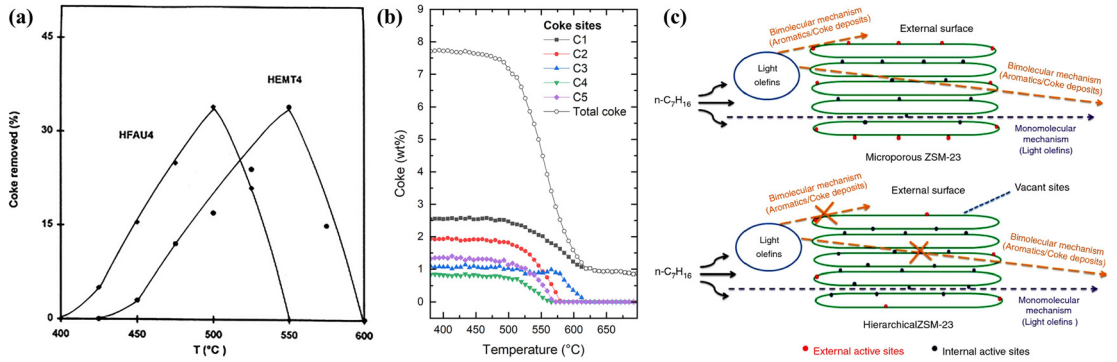

Fig. 7 (a) Oxidation of coke on HFAU4 and HEMT4 (coke content of about 10 wt%) *versus* temperature, reproduced from ref. 96 with permission from Elsevier, copyright 1998. (b) Evolution of the total coke and the individual coke occupancies within the H-ZSM-5 framework at increasing temperature for H-ZSM-5, reproduced from ref. 97 with permission from Royal Society of Chemistry, copyright 2022. (c) Proposed mechanism of *n*-heptane catalytic cracking over different active sites of ZSM-23 zeolites, reproduced from ref. 98 with permission from Springer Nature, copyright 2021.

sites,[96] as shown in Fig. 7a. The supercage structure of HFAU promotes external coke formation, facilitating oxidative removal, whereas the secondary cages (hypocages) of HEMT favor internal coke accumulation, thereby restricting oxygen access and slowing oxidation. These differences are attributed primarily to the pore topology, rather than the differences in chemical composition or acid strength.

Recent operando X-ray diffraction studies by Kalantzopoulos *et al.*[97] elucidated the regeneration behavior of coked H-ZSM-5 and revealed a two-step mechanism involving thermal decomposition of coke precursors around 475 °C, followed by oxidative removal of more rigid species between 530 and 620 °C. This process is accompanied by reversible deformation of the straight 10-membered ring channels, which recover from oval (coked) to near-circular (regenerated) shapes. Importantly, coke removal is site-dependent within the MFI framework: species residing in straight channels exhibit delayed removal and require higher oxidation temperatures (>575 °C), while those located at intersections and in zigzag channels are more readily oxidized at lower temperatures (~475–550 °C), as shown in Fig. 7b. Collectively, these observations confirm that framework topology is the dominant factor dictating coke oxidation dynamics.

Structural engineering can partially mitigate these topological limitations. For example, hierarchical ZSM-23 integrates secondary mesoporosity into its originally microporous framework, thereby enhancing oxygen diffusion and shifting coke deposition toward more accessible external sites,[98] as shown in Fig. 7c. As a result, it exhibits markedly lower activation energies for coke oxidation and superior preservation of internal acidity and crystallinity after deactivation compared to its purely microporous counterpart. These findings underscore the potential of hierarchical architectures to enhance the regeneration efficiency even within topologically constrained zeolite frameworks.

In addition to zeolite topology, the strength, density, and type (Brønsted or Lewis) of acid sites critically influence the catalytic performance, coke formation behavior, and the nature and reactivity of coke deposits during oxidative regeneration. Systematic studies on HY zeolites by Moljord *et al.*[99] revealed that a higher density of framework aluminum atoms, corresponding to increased Brønsted acid site concentration, facilitates coke oxidation, likely through proton-assisted molecular oxygen activation and the formation of a radical cation intermediate. Meanwhile, Díaz *et al.*[32] reported that in HZSM-5 catalysts, stronger acid sites associated with lower Si/Al ratios promote the formation of hard coke through secondary reactions such as dehydrogenation and aromatization; this coke requires harsher regeneration conditions (520–550 °C) with high activation energies (162–244 kJ mol^{-1}). Catalysts with weaker acid sites tend to form softer coke that can be removed by milder thermal treatment (~400 °C). Consistently, recent work by Jiang *et al.*[100] demonstrated that strong Lewis acid sites in Zr-β zeolites serve as primary sites for carbon deposition (Fig. 8), and their gradual loss correlating with catalyst deactivation. Regeneration under air at 450 °C effectively restored the Lewis acidity and catalytic activity, highlighting

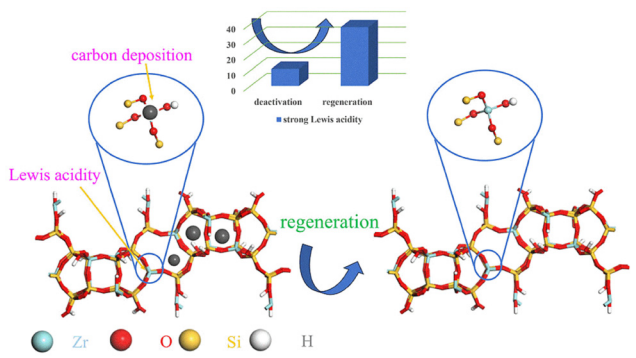

Fig. 8 Correlation between Lewis acid site distribution and coke deposition behavior over Zr-β zeolites during catalytic operation and regeneration, reproduced from ref. 100 with permission from American Chemical Society, copyright 2024.

the pivotal role of acid site strength in governing the coke reactivity and regeneration efficiency.

Coke oxidation is a highly exothermic process, and the resulting heat release poses a significant risk of catalyst degradation. Excessive local temperatures during regeneration may induce structural damage such as dealumination, framework collapse, and metal sintering, ultimately leading to irreversible loss of catalytic activity. Therefore, an ideal regeneration strategy must achieve complete coke removal while preserving the structural integrity and active sites of the catalyst. In industrial practice, key parameters such as regeneration temperature, oxygen concentration, and treatment duration must be carefully optimized to achieve this balance. Among these parameters, temperature plays a particularly critical role in determining both the kinetics of coke oxidation and the extent of catalyst recovery. Yung *et al.*[101] systematically examined the regeneration of coked ZSM-5 used in catalytic fast pyrolysis and found that a minimum temperature of 650 °C (Fig. 9a) was required to ensure effective coke removal and performance restoration. Lower temperatures led to incomplete decoking and extended regeneration times, whereas excessively high temperatures increased the risk of irreversible framework degradation and compromised the long-term durability. Oxygen concentration is similarly pivotal in controlling regeneration outcomes.[102,103] Akbari *et al.*[102] systematically investigated the regeneration of coked SAPO-34 in a fluidized-bed reactor and demonstrated that using 14 vol% O_2 at 600 °C achieved an optimal balance between efficient coke removal and the preservation of key catalyst properties, including strong acidity, microporosity, and structural integrity (Fig. 9b). These findings collectively underscore the necessity for precise tailoring of regeneration conditions to the physicochemical characteristics of each catalyst system to ensure both effective and safe performance recovery.

In addition to conventional oxidative regeneration using air or pure oxygen, alternative oxidants such as O_3 and NO_x have been explored to improve the coke removal efficiency at reduced temperatures, thereby mitigating catalyst structural degradation. O_3, with its high oxidative potential, enables effective coke oxidation at 150–200 °C, which is significantly lower than the temperatures typically required for O_2-based treatments.[104,105] For example, Copperthwaite *et al.*[104] restored the activity of coked ZSM-5 at 150 °C using ozone-enriched oxygen, while Mariey *et al.*[105] achieved nearly complete coke removal from HY zeolites at 180 °C. However, the industrial application of O_3 is limited by rapid decomposition, restricted diffusion, and stringent emission regulations.[94,106] Similarly, NO_x species such as N_2O and NO_2 can remove external coke at 350 to 400 °C, approximately 200 °C lower than conventional air-based regeneration.[107,108] Nevertheless, they may also induce framework degradation and aluminum redistribution, ultimately compromising the catalyst stability.[108] Consequently, although these alternative oxidants offer distinct advantages under mild regeneration conditions, their broader industrial adoption remains constrained by operational complexity, environmental concerns, and economic viability.

Gasification regeneration

Gasification regeneration refers to the conversion of coke deposits into syngas (CO and H_2) through reactions with carbon dioxide or steam.[109] Unlike conventional oxidative regeneration, which involves exothermic combustion and may induce local overheating and framework degradation, gasification is endothermic and allows greater thermal control. Two main gasification pathways are relevant in zeolite systems. Carbon dioxide gasification proceeds *via* the reverse Boudouard reaction ($C + CO_2 \rightarrow 2CO$, $\Delta H = +172$ kJ mol^{-1}), providing smoother temperature control but generally requiring high operating temperatures because of the low intrinsic reactivity of CO_2. In contrast, steam gasification ($C + H_2O \rightarrow CO + H_2$, $\Delta H = +131$ kJ mol^{-1}) exhibits significantly higher

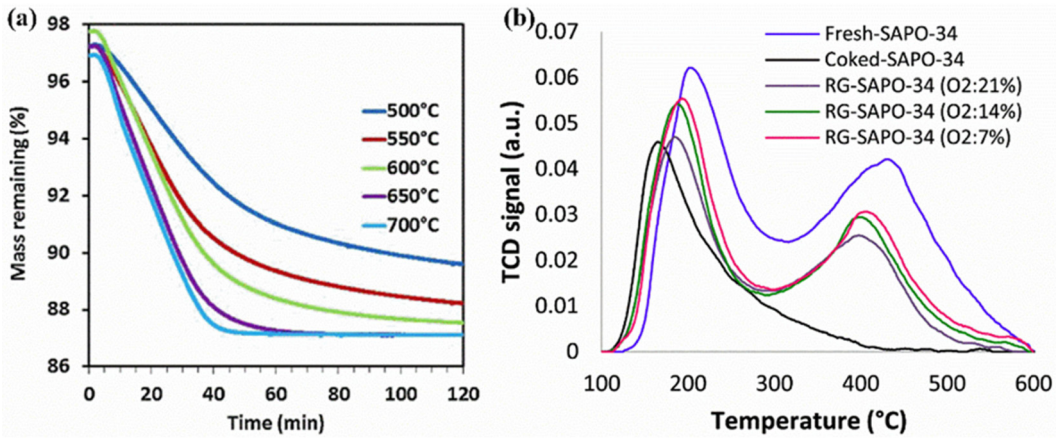

Fig. 9 (a) TGA profiles during the regeneration experiments with oxidative treatment in 4% O_2/N_2 at different temperatures, reproduced from ref. 101 with permission from Elsevier, copyright 2019. (b) NH_3-TPD spectrum of the fresh, spent, and different regenerated catalysts, reproduced from ref. 102 with permission from Elsevier, copyright 2024.

reactivity, typically two to five times higher under similar conditions.[109,110] However, steam introduces hydrothermal environments that can induce framework dealumination and aluminum migration, posing stability challenges for zeolite-based catalysts.

Several studies have demonstrated the feasibility of gasification-based regeneration for zeolite systems. Sun *et al.* achieved partial recovery of catalytic activity in FeLi/ZSM-5 ethylbenzene conversion catalysts following CO_2 gasification at 550 °C for four hours.[111] Karpe *et al.*[26] investigated the application of CO_2 gasification regeneration for the deactivated Fe-ZSM-5 catalyst in the methane MDA reaction. Their results show that regeneration at 830 °C effectively removed soft carbon species, whereas higher temperatures (860 °C) are required for complete elimination of hard coke, confirming the temperature-dependent nature of CO_2 gasification.

For steam gasification applications, Zhang *et al.*[112] developed bifunctional catalysts by modifying USY zeolites with alkaline metal oxides, achieving a 50% reduction in regeneration time compared to conventional air-based methods. Notably, Zhou *et al.*[113] demonstrated that controlled partial steam regeneration of SAPO-34 catalysts in methanol-to-olefins processes could preserve beneficial coke species, resulting in enhanced ethylene selectivity compared to complete coke removal. These examples illustrate how both complete and partial regeneration strategies can be tailored to balance the activity recovery and selectivity.

While gasification-based regeneration offers advantages such as improved thermal control and potential coke valorization, it also faces significant limitations. Both CO_2 gasification (typically >700 °C) and steam gasification (commonly 700–900 °C) require high operating temperatures, which can degrade the zeolite crystallinity and compromise the acid site stability. Although steam possesses higher intrinsic reactivity than CO_2, achieving complete coke removal often necessitates even more severe thermal conditions. Moreover, the regeneration efficiency is highly sensitive to catalyst composition, coke characteristics, and reaction parameters. Compared to oxidative regeneration, gasification provides a gentler alternative, particularly suitable when structural preservation and gradual coke removal are desired.

Non-oxidative regeneration

Non-oxidative regeneration refers to coke removal processes that avoid the use of oxygen or strong oxidants, relying instead on alternative pathways such as thermal cracking, hydrogenation, or chemical reduction. Representative methods include pyrolysis under inert atmospheres (*e.g.*, N_2), hydrocracking using hydrogen or alkanes, and other reductive treatments.[114–117] These approaches are particularly advantageous for catalysts that are susceptible to framework degradation under oxidative conditions.

Among these strategies, hydrogenation is the most extensively studied method for regenerating zeolite-based catalysts. The primary reaction involves the hydrogenation of carbonaceous deposits to methane: $C(s) + 2H_2(g) \rightarrow CH_4(g)$, $\Delta H = -75$ kJ mol^{-1}.[118] The efficiency of hydrogen-based regeneration depends strongly on both the physicochemical properties of the catalyst and the operating parameters. Bauer *et al.*[114] reported that spent HZSM-5 catalysts used in methanol-to-hydrocarbon reactions could be partially reactivated using hydrogen or alkanes around 420 °C, attributed to Brønsted acid sites that activate hydrogen and promote coke hydrocracking.

Similarly, Aguayo *et al.*[115] examined the regeneration of coke-laden HZSM-5 zeolites using helium, hydrogen, and water vapor. Helium lowered the coke content and its H/C ratio but only transiently restored activity, with rapid deactivation in subsequent reactions. Hydrogen, in contrast, reduced and stabilized the coke deposits, thereby decreasing the subsequent deactivation rate and acting as an ideal regenerant. Water vapor partially removed coke but caused aluminum leaching and acid-site loss, leading to irreversible deactivation and poor catalytic durability. Thus, hydrogen treatment was considered the most effective option for HZSM-5 regeneration, as it effectively removes coke, stabilizes activity, and prolongs service life. Jong *et al.*[119] further showed that coke located near these acid sites was more readily removed than on the external surface, indicating the spatial selectivity of hydrogen activation. For Mo/HZSM-5 catalysts used in MDA, effective regeneration required temperatures above 850 °C,[120] while elevated hydrogen pressures (up to 4 MPa) significantly improved coke removal in SAPO-34 systems.[121]

Despite these advantages, hydrogenation remains less efficient than oxidative routes and generally demands high temperatures and/or pressures to achieve appreciable coke conversion. Walker *et al.*[122] reported coke removal rates at 800 °C in the order $O_2 > H_2O > CO_2 > H_2$, confirming the relatively low reactivity of hydrogenation. Nevertheless, hydrogen treatment offers unique advantages, including the preferential removal of internal coke near Brønsted acid sites while retaining some external carbon deposits that may contribute to shape selectivity or catalyst protection.[123]

Non-thermal plasma regeneration

In response to the limitations of conventional thermal regeneration methods, a growing number of alternative technologies have been proposed to improve the efficiency and selectivity of catalyst regeneration. Among these, non-thermal plasma regeneration has emerged as a particularly promising strategy for coked zeolite catalysts.[30,124] Unlike traditional oxidative regeneration that relies on high-temperature combustion (typically >500 °C), NTP enables catalyst regeneration at room temperature and atmospheric pressure by generating highly reactive oxygen species, such as O_2^+, O^-, O_2^-, and O_3, through electron impact excitation in oxygen-containing plasma environments. A typical dielectric barrier discharge (DBD) reactor configuration used for this purpose is illustrated in Fig. 10a.[125]

These reactive species exhibit strong oxidative activity and are capable of diffusing into the microporous network of zeolites,[126] including pores smaller than 1 nanometer (Fig. 10b). The decoking process is primarily governed by the density and

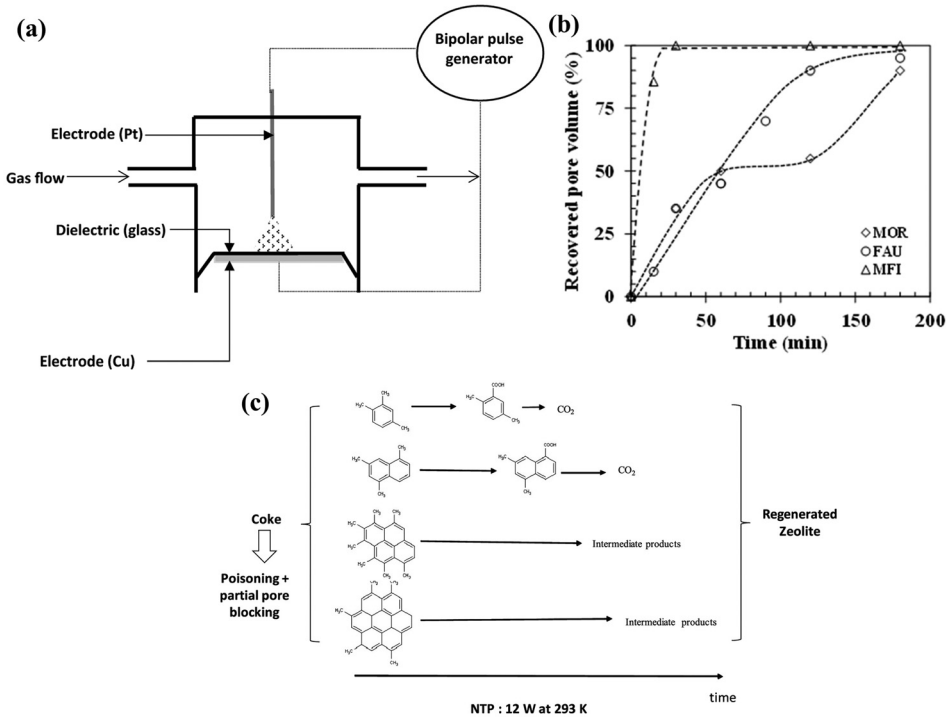

Fig. 10 (a) Schematic of a typical dielectric barrier discharge reactor used for NTP regeneration, reproduced from ref. 125 with permission from Springer Nature, copyright 2019. (b) Percentage of microporous volume regenerated on MOR, FAU and MFI zeolites as a function of regeneration time for 12 W at 293 K, reproduced from ref. 126 with permission from MDPI, copyright 2019. (c) Apparent oxidation path of coke by NTP regeneration, reproduced from ref. 127 with permission from American Chemical Society, copyright 2019.

mobility of these species, allowing selective oxidation of polyaromatic coke molecules confined within the zeolite framework. Mechanistically, coke elimination occurs *via* a stepwise oxidation sequence: lighter hydrocarbons are oxidized first, while more condensed aromatic deposits undergo partial oxidation to form carboxylic intermediates, which subsequently desorb as volatile organic compounds such as CO and CO_2.[127] This mechanism is schematically depicted in Fig. 10c. The low-temperature and selective oxidation pathway enables effective coke removal while minimizing structural degradation and framework dealumination.

Experimental studies have demonstrated the applicability of NTP regeneration across various zeolite structures, including MFI-, FAU-, and MOR-type zeolites. For instance, MFI and FAU zeolites can be almost completely regenerated within a few hours under DBD plasma conditions, with restoration of microporosity and acidity. In contrast, MOR zeolites show slower regeneration due to their more restrictive channel systems.[126] A comparison of regeneration performances among different zeolite types is presented in Fig. 10b. The efficiency of NTP regeneration also strongly depends on both the chemical nature of the coke species and the physical compactness of the catalyst bed, which influence the accessibility and reactivity of plasma-generated species within the porous network.

NTP provides a selective, energy-efficient, and structure-preserving method for the regeneration of coked zeolites, offering great promise for extending the catalyst lifetime in hydrocarbon conversion processes. However, as a relatively new technique, its industrial application still faces several challenges, including the high cost associated with the use of noble gas mixtures such as He or Ar to stabilize the discharge and the need for optimized reactor configurations to ensure effective plasma–catalyst interactions and scalability.

Summary and outlook

Coke-induced deactivation remains the foremost challenge limiting the long-term performance of zeolite catalysts in industrial petrochemical and refining processes. This review summarizes the recent advances in understanding coke formation and deactivation mechanisms, discusses strategies for mitigating coking through zeolite modification, and evaluates a range of regeneration technologies.

The underlying mechanisms are highly complex and are intrinsically governed by the interplay among framework topology, acidity distribution, and reaction environment, which together determine the location, chemistry, and growth dynamics of carbonaceous species. Despite the considerable recent progress, fundamental questions remain regarding the molecular-level mechanisms that control coke nucleation, growth, and spatial evolution under realistic reaction conditions. Current understanding relies heavily on *ex situ* charac-

terization, which provides limited insight into the multiscale and dynamic nature of these processes. A systematic investigation of carbon deposition pathways, the structural and diffusional behavior of coke precursors and deposits, and their interactions with active sites is urgently needed. The integration of density functional theory, molecular dynamics simulations, microkinetic modeling, and advanced experiments offers powerful opportunities to establish predictive structure–coking relationships, deepen the mechanistic understanding across multiple length and time scales, and guide the design of multifunctional zeolite catalysts with enhanced resistance to deactivation.

The rational design of coke-resistant zeolite catalysts has traditionally proceeded through iterative experimental optimization, which is inherently resource-intensive. It is constrained by a vast parameter space, including framework topology, Si/Al ratio, metal incorporation strategies, acidity modification, and hierarchical structuring techniques, as summarized in this work. In recent years, artificial intelligence (AI) and computational screening methodologies have emerged as transformative tools in zeolite materials science, offering unprecedented capabilities across the complete design–synthesis–characterization pipeline.[128–132] These AI-driven approaches have been successfully applied to framework identification, thermodynamic stability assessment, adsorption performance prediction, hypothetical structure generation, and experimental synthesis pathway design.[132] Nevertheless, applications specifically targeting the anti-coking performance remain at an early stage, largely due to the complex, multi-factorial nature of catalyst deactivation and the fragmented, heterogeneous datasets available in the literature. In the future, by processing large, standardized, high-quality datasets from experimental and operational conditions, AI-enabled zeolite screening and process optimization hold the potential to enable predictive analysis of coke formation, guide informed catalyst design,[133,134] and implement advanced process control strategies[47] for the rational development of coke-resistant zeolite catalysis systems.

Regeneration strategies involve a fundamental trade-off between decoking efficiency and structural preservation, as summarized in this review. Oxidative regeneration with O_2 remains the industrial standard due to its high kinetic efficiency and scalability, though its highly exothermic nature necessitates careful thermal management to prevent dealumination, framework collapse, and metal sintering over repeated cycles. Low-temperature alternatives, such as O_3, NO_x, and non-thermal plasma, significantly mitigate structural risks but are constrained by economic and scalability limitations. Gasification with CO_2 or H_2O offers improved thermal control through endothermic pathways and enables potential syngas valorization, though high temperatures may compromise zeolite crystallinity; steam, while more reactive than CO_2, can induce hydrothermal instability and acid site loss. Hydrogenation, although the least efficient, selectively removes internal coke while preserving external carbon layers that contribute to shape selectivity. Optimal regeneration strategies should be tailored to operational priorities: high-throughput processes favor conventional oxidative regeneration with optimized temperature and oxygen concentration, whereas structure-sensitive applications benefit from low-temperature methods. Future efforts should focus on integrating the efficiency of thermal regeneration with the structural preservation offered by low-temperature approaches.

Future progress in overcoming coke-induced deactivation in zeolite catalysts will rely on a concerted, multidisciplinary effort integrating advanced characterization, multiscale modeling, data science, and reaction engineering. Several research directions deserve particular emphasis. First, *in situ* and operando characterization techniques capable of capturing the spatiotemporal evolution of coke under realistic reaction–regeneration conditions remain less developed, yet they are indispensable for validating mechanistic hypotheses and developing rational catalyst design. Second, computational approaches ranging from quantum chemical calculations of confined reaction pathways to data-driven structure–property modeling need further development. Closer integration with experiments is also required to fully realize their potential for accelerating catalyst discovery and optimization. Third, novel low-energy, low-emission regeneration techniques should be tailored to target specific deactivation pathways, ensuring they are both efficient and sustainable. By integrating molecular-level mechanistic insights, rational design strategies, advanced characterization, and sustainable regeneration technologies, significant advances can be achieved in the design and optimization of durable zeolite catalysts.

Author contributions

Conceptualization, Z. Z.; writing – original draft preparation, M. Z., F. M., J. H. and C. Z.; writing – review and editing, Z. Z.; supervision, Z. Z. and C. Z.; funding acquisition, Z. Z. All authors have read and agreed to the published version of the manuscript.

Conflicts of interest

The authors declare no conflicts of interest.

Data availability

No primary research results, software or code have been included and no new data were generated or analysed as part of this review.

Acknowledgements

This work was financially supported by the National Key Research and Development Program of China (2024YFB4006400).

References

1 Y. Li and J. Yu, *Nat. Rev. Mater.*, 2021, **6**, 1156–1174.
2 M. H. M. Sofi, M. Y. S. Hamid, A. A. Jalil, A. Alhebshi, N. S. Hassan, M. B. Bahari and M. Y. Mohamud, *Arabian J. Sci. Eng.*, 2025, **50**, 3671–3697.
3 L. Wang, X. Gao, Y. Qu, Y. Diao and H. Song, *Fuel*, 2025, **384**, 133957.
4 D. J. Mihalcik, C. A. Mullen and A. A. Boateng, *J. Anal. Appl. Pyrolysis*, 2011, **92**, 224–232.
5 M. Cheng, H. Cruchade, L. Pinard, E. Dib, H. Liu, J. Wang, X. Liu, Z.-F. Yan, Z. Qin and S. Mintova, *J. Mater. Chem. A*, 2023, **11**, 24991–24998.
6 J. H. Harrhy, A. Wang, J. S. Jarvis, P. He, S. Meng, M. Yung, L. Liu and H. Song, *Commun. Chem.*, 2019, **2**, 37.
7 V. Daligaux, R. Richard and M.-H. Manero, *Catalysts*, 2021, **11**, 770.
8 F. Wang, P. Wang, J. Zhang, D. Peng, M. Wei and D. Zhang, *Chin. Chem. Lett.*, 2024, **35**, 108800.
9 Y. Xie, Y. Zhang, L. He, C. Q. Jia, Q. Yao, M. Sun and X. Ma, *Appl. Catal., A*, 2023, **657**, 119159.
10 D. Chen, K. Moljord and A. Holmen, *Microporous Mesoporous Mater.*, 2012, **164**, 239–250.
11 A. Zabihpour, J. Ahmadpour and F. Yaripour, *Chem. Eng. Sci.*, 2023, **273**, 118639.
12 J. Ma, S. Chang, F. Yu, H. Lai and Y. Zhao, *Catalysts*, 2022, **12**, 1499.
13 S. Fan, H. Wang, S. Wang, M. Dong and W. Fan, *Sci. China: Chem.*, 2024, **67**, 3934–3943.
14 Y. Sun, L. Wei, Z. Zhang, H. Zhang and Y. Li, *Energy Fuels*, 2023, **37**, 1657–1677.
15 J. Zhou, J. Zhao, J. Zhang, T. Zhang, M. Ye and Z. Liu, *Chin. J. Catal.*, 2020, **41**, 1048–1061.
16 M. Xu, C. Mukarakate, D. J. Robichaud, M. R. Nimlos, R. M. Richards and B. G. Trewyn, *Top. Catal.*, 2016, **59**, 73–85.
17 A. Hwang and A. Bhan, *Acc. Chem. Res.*, 2019, **52**, 2647–2656.
18 D. Chen, Z. Sheng, S. Huang, H. Huang, Y. Zhong, K. Zhuang, Y. Zhang and L. Yang, *Mol. Catal.*, 2025, **584**, 115274.
19 A. Kostyniuk, D. Bajec, A. Prašnikar and B. Likozar, *J. Ind. Eng. Chem.*, 2021, **101**, 293–306.
20 R. L. Mortensen, H.-D. Noack, K. Pedersen, S. Mossin and J. Mielby, *ChemCatChem*, 2022, **14**, e202101924.
21 M. Jindal, V. C. S. Palla and B. Thallada, *Bioresour. Technol.*, 2023, **376**, 128933.
22 L.-H. Chen, M.-H. Sun, Z. Wang, W. Yang, Z. Xie and B.-L. Su, *Chem. Rev.*, 2020, **120**, 11194–11294.
23 X. Zhu, N. Kosinov, J. P. Hofmann, B. Mezari, Q. Qian, R. Rohling, B. M. Weckhuysen, J. Ruiz-Martínez and E. J. M. Hensen, *Chem. Commun.*, 2016, **52**, 3227–3230.
24 M. Moliner, C. Martínez and A. Corma, *Angew. Chem., Int. Ed.*, 2015, **54**, 3560–3579.
25 L. Oar-Arteta, A. Remiro, J. Vicente, A. T. Aguayo, J. Bilbao and A. G. Gayubo, *Fuel Process. Technol.*, 2014, **126**, 145–154.
26 S. Karpe and G. Veser, *Catalysts*, 2024, **14**, 292.
27 H. Zhang, Z. Shen, J. Gong and H. Liu, *Chin. J. Chem. Eng.*, 2023, **63**, 71–80.
28 A. Benamar, Z. Bechket, Y. Boucheffa and A. Miloudi, *C. R. Chim.*, 2009, **12**, 706–715.
29 S. Shao, Z. Ye, J. Sun, C. Liu, J. Yan, T. Liu, X. Li, H. Zhang and R. Xiao, *Fuel*, 2022, **330**, 125420.
30 L. Pinard and C. Batiot-Dupeyrat, *Catal. Today*, 2024, **426**, 114372.
31 I. M. S. Anekwe and Y. M. Isa, *Energy Adv.*, 2025, **4**, 1075–1113.
32 M. Díaz, E. Epelde, J. Valecillos, S. Izaddoust, A. T. Aguayo and J. Bilbao, *Appl. Catal., B*, 2021, **291**, 120076.
33 Z. Wan, W. Wu, G. Li, C. Wang, H. Yang and D. Zhang, *Appl. Catal., A*, 2016, **523**, 312–320.
34 S. P. Bedenko, K. I. Dement'ev and V. F. Tret'yakov, *Catalysts*, 2021, **11**, 1181.
35 P. Castaño, G. Elordi, M. Olazar, A. T. Aguayo, B. Pawelec and J. Bilbao, *Appl. Catal., B*, 2011, **104**, 91–100.
36 P. Rzepka, D. Sheptyakov, C. Wang, J. A. van Bokhoven and V. Paunović, *ACS Catal.*, 2024, **14**, 5593–5604.
37 M. Migliori, E. Catizzone, A. Aloise, G. Bonura, L. Gómez-Hortigüela, L. Frusteri, C. Cannilla, F. Frusteri and G. Giordano, *J. Ind. Eng. Chem.*, 2018, **68**, 196–208.
38 J. T. C. Wennmacher, S. Mahmoudi, P. Rzepka, S. Sik Lee, T. Gruene, V. Paunović and J. A. van Bokhoven, *Angew. Chem., Int. Ed.*, 2022, **61**, e202205413.
39 J. Fals, M. L. Ospina-Castro, A. Ramos-Hernández, L. Pacheco-Londoño and S. Bocanegra, *Heliyon*, 2024, **10**, e37813.
40 J. Fals, C. A. T. Toloza, E. Puello-Polo, E. Márquez and F. J. Méndez, *Heliyon*, 2023, **9**, e15408.
41 J. Fals, J. F. Garcia-Valencia, E. Puello-Polo, F. Tuler and E. Márquez, *Molecules*, 2024, **29**, 3085.
42 J. Fals, E. Puello-Polo and E. Márquez, *Molecules*, 2024, **29**, 4753.
43 A. Ochoa, J. Bilbao, A. G. Gayubo and P. Castaño, *Renewable Sustainable Energy Rev.*, 2020, **119**, 109600.
44 Y. Gao, S.-L. Chen, Y. Wei, Y. Wang, W. Sun, Y. Cao and P. Zeng, *Chem. Eng. J.*, 2017, **326**, 528–539.
45 L. Zhou, H. Zhao, Y. Tong, J. Gao, X. Hao, Y. Yang and Y. Li, *Ind. Eng. Chem. Res.*, 2022, **61**, 17440–17456.
46 O. Singh, A. V. Ramteke, B. Joshi, B. P. Vempatapu, K. K. Pant, A. Ray and B. Sarkar, *ACS Sustainable Chem. Eng.*, 2023, **11**, 17061–17074.
47 Z. M. Shakor and E. N. Al-Shafei, *RSC Adv.*, 2023, **13**, 22579–22592.
48 T. Cordero-Lanzac and J. Bilbao, *Chem. Eng. J.*, 2025, **514**, 162856.
49 C. W. P. Pare, P. Rzepka, P. Hemberger, A. Bodi, R. Hauert, J. A. van Bokhoven and V. Paunović, *ACS Catal.*, 2024, **14**, 463–474.
50 S. Zhou, S. Tang, G. Li, S. Xin, F. Huang, X. Liu, T. Mi, K. Huang and L. Zeng, *Fuel*, 2023, **333**, 126311.
51 Q. Zhang, S. Gao and J. Yu, *Chem. Rev.*, 2023, **123**, 6039–6106.

52 B. Zhang, M. Song, M. Xu and G. Liu, *Energy Fuels*, 2023, **37**, 19419–19432.
53 A. Zeinali Varzaneh, J. Towfighi and M. Saei Moghaddam, *React. Kinet., Mech. Catal.*, 2019, **128**, 1043–1063.
54 X. Jiang, X. Su, X. Bai, Y. Li, L. Yang, K. Zhang, Y. Zhang, Y. Liu and W. Wu, *Microporous Mesoporous Mater.*, 2018, **263**, 243–250.
55 M. Sedighi, M. Ghasemi, M. Sadeqzadeh and M. Hadi, *Powder Technol.*, 2016, **291**, 131–139.
56 N.-Y. Yao, J.-P. Cao, X.-Y. Zhao, X.-B. Pang, J.-P. Zhao, C.-X. Chen, S.-J. Cai, X.-B. Feng and D. Dung Le, *J. Anal. Appl. Pyrolysis*, 2024, **179**, 106516.
57 I. M. S. Anekwe, B. Oboirien and Y. M. Isa, *Fuel Commun.*, 2024, **18**, 100101.
58 A. Sridhar, M. Rahman, A. Infantes-Molina, B. J. Wylie, C. G. Borcik and S. J. Khatib, *Appl. Catal., A*, 2020, **589**, 117247.
59 H. Han, A. Zhang, L. Ren, X. Nie, M. Liu, Y. Liu, C. Shi, H. Yang, C. Song and X. Guo, *Chem. Eng. Sci.*, 2022, **252**, 117529.
60 B. Joshi, S. Singhal, A. K. Yadav, B. Vempatapu, A. Agarwal, N. Gopinathan, O. Singh and B. Sarkar, *ChemCatChem*, 2025, **17**, e00424.
61 J. Zhang, F. Yuan, A. Zhang, G. Zhang, L. Ren, C. Song and X. Guo, *Fuel*, 2024, **357**, 129904.
62 S. Ma, Z. Zhang, H. Zhao, Y. Hu, B. Avid and S. Xue, *J. Anal. Appl. Pyrolysis*, 2025, **192**, 107282.
63 H. Khezri, A. Izadbakhsh and A. A. Izadpanah, *Fuel Process. Technol.*, 2020, **199**, 106253.
64 J. Lu, Z. Xu, Y. Yue, X. Bao, M. Lin and H. Zhu, *Chem. Eng. J.*, 2024, **484**, 149369.
65 J. Zhou, H. Liu, C. Xiong, P. Hu, H. Wang, X. Wang and H. Ji, *Chem. Eng. J.*, 2023, **455**, 139794.
66 Y. Wang, Y. Suo, X. Lv, Z. Wang and Z.-Y. Yuan, *J. Colloid Interface Sci.*, 2021, **593**, 304–314.
67 S. V. Konnov, F. Dubray, E. B. Clatworthy, C. Kouvatas, J.-P. Gilson, J.-P. Dath, D. Minoux, C. Aquino, V. Valtchev, S. Moldovan, S. Koneti, N. Nesterenko and S. Mintova, *Angew. Chem., Int. Ed.*, 2020, **59**, 19553–19560.
68 Y. Gu, P. Chen, X. Wang, Y. Lyu, W. Liu, X. Liu and Z. Yan, *ACS Catal.*, 2021, **11**, 6771–6786.
69 I. M. S. Anekwe, M. Chetty, L. Khotseng, S. L. Kiambi, L. Maharaj, B. Oboirien and Y. M. Isa, *Catal. Commun.*, 2024, **186**, 106802.
70 S. H. Bakhtiar, A. Ismail, S. Ali, F. Raziq, S. A. Hussain, A. Zada, W. Dong, M. Zahid and Q. Fu, *Inorg. Chem. Commun.*, 2024, **159**, 111835.
71 G. Ferrarelli, M. Migliori and E. Catizzone, *ACS Omega*, 2024, **9**, 29072–29087.
72 Z. Pan, A. Puente-Urbina, S. R. Batool, A. Bodi, X. Wu, Z. Zhang, J. A. van Bokhoven and P. Hemberger, *Nat. Commun.*, 2023, **14**, 4512.
73 J. Shan, Z. Li, Z. Chen, D. Wang, X. Zhang, Z. Ning, Y. Xue and S. Zhu, *Chem. Eng. J.*, 2023, **460**, 141741.
74 M. A. Sanhoob, G. A. Nasser, A. I. Bakare, O. Muraza, T. K. Al-Shammari, H. V. Lee, T. Yokoi, S. Park and T. Nishitoba, *Arabian J. Sci. Eng.*, 2023, **48**, 16483–16494.
75 H.-w. Huang, H. Zhu, S.-h. Zhang, Q. Zhang and C.-y. Li, *J. Fuel Chem. Technol.*, 2019, **47**, 74–82.
76 P. Degirmencioglu and H. Arbag, *Arabian J. Sci. Eng.*, 2023, **48**, 16123–16136.
77 Y. Gan, Q. Lv, Y. Li, H. Yang, K. Xu, L. Wu, Y. Tang and L. Tan, *Chem. Eng. Sci.*, 2023, **266**, 118289.
78 L. Song, J. C. Navarro de Miguel, S. Komaty, S.-H. Chung and J. Ruiz-Martínez, *ACS Catal.*, 2025, **15**, 5623–5639.
79 H. E. van der Bij and B. M. Weckhuysen, *Chem. Soc. Rev.*, 2015, **44**, 7406–7428.
80 S. Lee, C.-U. Kim, J.-C. Kim, S.-U. Lee, J. H. Kwak, R. Ryoo and T.-W. Kim, *Chem. Eng. J.*, 2022, **446**, 137169.
81 E. N. Al-Shafei, A. Masudi, Z. H. Yamani and O. Muraza, *ACS Omega*, 2022, **7**, 30807–30815.
82 I. Alalq, A. C. Jerdy, H. Nguyen-Phu, A. Zornes, M. Wulfers, D. Nielsen, D. Resasco, J. L. White and S. Crossley, *J. Catal.*, 2025, **447**, 116096.
83 Z. Xu, Y. Zhu, N. Jiao, K. Shi and H. Wang, *ACS Catal.*, 2025, **15**, 4618–4633.
84 P. Peng, X.-H. Gao, Z.-F. Yan and S. Mintova, *Natl. Sci. Rev.*, 2020, **7**, 1726–1742.
85 D. Kerstens, B. Smeyers, J. Van Waeyenberg, Q. Zhang, J. Yu and B. F. Sels, *Adv. Mater.*, 2020, **32**, 2004690.
86 M. Choi, K. Na, J. Kim, Y. Sakamoto, O. Terasaki and R. Ryoo, *Nature*, 2009, **461**, 246–249.
87 Y.-L. Zhu, H. Dai, Y. Duan, Q. Chen and M. Zhang, *Cryst. Growth Des.*, 2020, **20**, 2623–2631.
88 J. Wu, M. Dai, B. Yang, P. Li, C. Wang, G. Wu, X. Jiang, S. Yu, W. Li, X. Li, T. Zhao, D. Yang, R. Chu and X. Meng, *Chem. Eng. J.*, 2024, **482**, 148947.
89 J. Li, X. Li, G. Zhou, W. Wang, C. Wang, S. Komarneni and Y. Wang, *Appl. Catal., A*, 2014, **470**, 115–122.
90 C. Sun, A. Zhao, Y. Wang, Z. Wang, J. Zhao, T. Zhao, W. Liu, M. Shi, J. Lu, S. Wu and L. Bu, *Microporous Mesoporous Mater.*, 2021, **310**, 110619.
91 G. Wu, Q. Bao, J. Zhang, M. Luo, Z. Chen, X. Qiao, Y. Hu, W. Wang and Y. Hu, *Catal. Sci. Technol.*, 2025, **15**, 1003–1008.
92 X. Guo, Y. Zheng, B. Zhang and J. Chen, *Biomass Bioenergy*, 2009, **33**, 1469–1473.
93 P. Tian, Y. Wei, M. Ye and Z. Liu, *ACS Catal.*, 2015, **5**, 1922–1938.
94 L. Y. Jia, A. Farouha, L. Pinard, S. Hedan, J. D. Comparot, A. Dufour, K. Ben Tayeb, H. Vezin and C. Batiot-Dupeyrat, *Appl. Catal., B*, 2017, **219**, 82–91.
95 P. Magnoux and M. Guisnet, *Appl. Catal.*, 1988, **38**, 341–352.
96 G. A. Doka Nassionou, P. Magnoux and M. Guisnet, *Microporous Mesoporous Mater.*, 1998, **22**, 389–398.
97 G. N. Kalantzopoulos, D. Rojo Gama, D. K. Pappas, I. Dovgaliuk, U. Olsbye, P. Beato, L. F. Lundegaard, D. S. Wragg and S. Svelle, *Dalton Trans.*, 2022, **51**, 16845–16851.
98 B. J. B. Silva, L. V. Sousa, L. R. A. Sarmento, A. C. S. Melo, D. S. Silva, P. H. L. Quintela, S. L. Alencar and

A. O. S. Silva, *J. Therm. Anal. Calorim.*, 2021, **147**, 3161–3170.
99 K. Moljord, P. Magnoux and M. Guisnet, *Catal. Lett.*, 1994, **25**, 141–147.
100 H. Jiang, H. Zhao, S. Jiang, L. Wang and G. Yang, *Ind. Eng. Chem. Res.*, 2024, **63**, 21771–21779.
101 M. M. Yung, A. K. Starace, M. B. Griffin, J. D. Wells, R. E. Patalano, K. R. Smith and J. A. Schaidle, *Catal. Today*, 2019, **323**, 76–85.
102 A. Akbari, H. Haji Andevary and M. Omidkhah, *Chem. Eng. Process. – Process Intensif.*, 2024, **201**, 109821.
103 L. Zhang, Z. Bao, S. Xia, Q. Lu and K. B. Walters, *Catalysts*, 2018, **8**, 659.
104 R. G. Copperthwaite, G. J. Hutchings, P. Johnston and S. W. Orchard, *J. Chem. Soc., Faraday Trans. 1*, 1986, **82**, 1007–1017.
105 L. Mariey, J. Lamotte, T. Chevreau and J. C. Lavalley, *React. Kinet. Catal. Lett.*, 1996, **59**, 241–246.
106 R. Richard, C. Julcour and M.-H. Manero, *Ozone: Sci. Eng.*, 2017, **39**, 366–373.
107 D. P. Ivanov, V. I. Sobolev and G. I. Panov, *Appl. Catal., A*, 2003, **241**, 113–121.
108 K. Barbera, S. Sørensen, S. Bordiga, J. Skibsted, H. Fordsmand, P. Beato and T. V. W. Janssens, *Catal. Sci. Technol.*, 2012, **2**, 1196–1206.
109 G. Tian, G. Wang, C. Xu and J. Gao, *Ind. Eng. Chem. Res.*, 2013, **52**, 16737–16744.
110 M. F. Irfan, M. R. Usman and K. Kusakabe, *Energy*, 2011, **36**, 12–40.
111 A. Sun, Z. Qin and J. Wang, *Appl. Catal., A*, 2002, **234**, 179–189.
112 Y. Zhang, D. Yu, W. Li, S. Gao and G. Xu, *Fuel*, 2014, **117**, 1196–1203.
113 J. Zhou, J. Zhang, Y. Zhi, J. Zhao, T. Zhang, M. Ye and Z. Liu, *Ind. Eng. Chem. Res.*, 2018, **57**, 17338–17347.
114 F. Bauer, H. Ernst, E. Geidel and R. Schödel, *J. Catal.*, 1996, **164**, 146–151.
115 A. T. Aguayo, A. G. Gayubo, J. Ereña, A. Atutxa and J. Bilbao, *Ind. Eng. Chem. Res.*, 2003, **42**, 3914–3921.
116 P. Magnoux, H. S. Cerqueira and M. Guisnet, *Appl. Catal., A*, 2002, **235**, 93–99.
117 R. Klingmann, R. Josl, Y. Traa, R. Gläser and J. Weitkamp, *Appl. Catal., A*, 2005, **281**, 215–223.
118 P. Marecot, S. Peyrovi, D. Bahloul and J. Barbier, I. Regeneration of precoked catalysts, *Appl. Catal.*, 1990, **66**, 181–190.
119 S.-J. Jong, A. R. Pradhan, J.-F. Wu, T.-C. Tsai and S.-B. Liu, *J. Catal.*, 1998, **174**, 210–218.
120 S. J. Han, S. K. Kim, A. Hwang, S. Kim, D.-Y. Hong, G. Kwak, K.-W. Jun and Y. T. Kim, *Appl. Catal., B*, 2019, **241**, 305–318.
121 X. Zhao, J. Li, P. Tian, L. Wang, X. Li, S. Lin, X. Guo and Z. Liu, *ACS Catal.*, 2019, **9**, 3017–3025.
122 P. L. Walker, S. Matsumoto, T. Hanzawa, T. Muira and I. M. K. Ismail, *Fuel*, 1983, **62**, 140–149.
123 F. Bauer, W.-H. Chen, Q. Zhao, A. Freyer and S.-B. Liu, *Microporous Mesoporous Mater.*, 2001, **47**, 67–77.
124 Y. Fan, G. Hou, Y. Xiong, C. Chen and W. Zhao, *Catal. Sci. Technol.*, 2020, **10**, 7965–7983.
125 L. Pinard, N. Ayoub and C. Batiot-Dupeyrat, *Plasma Chem. Plasma Process.*, 2019, **39**, 929–936.
126 A. Astafan, A. Sachse, C. Batiot-Dupeyrat and L. Pinard, *Catalysts*, 2019, **9**, 985.
127 A. Astafan, C. Batiot-Dupeyrat and L. Pinard, *J. Phys. Chem. C*, 2019, **123**, 9168–9175.
128 Z. Jensen, E. Kim, S. Kwon, T. Z. H. Gani, Y. Román-Leshkov, M. Moliner, A. Corma and E. Olivetti, *ACS Cent. Sci.*, 2019, **5**, 892–899.
129 X. Li, H. Han, N. Evangelou, N. J. Wichrowski, P. Lu, W. Xu, S.-J. Hwang, W. Zhao, C. Song, X. Guo, A. Bhan, I. G. Kevrekidis and M. Tsapatsis, *Nat. Commun.*, 2023, **14**, 3152.
130 Q.-C. Zhao, L. Chen, S. Ma and Z.-P. Liu, *Nat. Commun.*, 2025, **16**, 3720.
131 L. Li, X. Xu, M. Ye and Z. Liu, *J. Phys. Chem. C*, 2025, **129**, 24–36.
132 M. Wu, S. Zhang and J. Ren, *APL Mater.*, 2025, **13**, 020601.
133 A. Pourian, A. Rahmanifard, S. Maghsoudy, M. T. Verki, M. Salami-Kalajahi and S. Habibzadeh, *J. Mater. Chem. A*, 2025, **13**, 30554–30575.
134 Y. Ye, B. Bai, Y. Ding, X. Li, F. Jiao, J. Xiao and X. Pan, *Angew. Chem., Int. Ed.*, 2025, **64**, e202505589.